Engineering and Technology Journal 43 (12) (2025) 1051-1065

Engineering and Technology Journal
Journal homepage: https://etj.uotechnology.edu.iq

Impact of sintering time on corrosion rate and relative density of titanium, titanium-aluminum alloy, and titanium-based composites for bio-applications

Marwa Hadi*, Niveen J. Abdulkader, Layth W. Al-Gebory

Materials Engineering Dept., University of Technology-Iraq, Alsina'a street, 10066 Baghdad, Iraq.
*Corresponding author Email: mae.22.040@grad.uotechnology.edu.iq

HIGHLIGHTS

- A novel Ti-Al-HA composite was developed for bone plate fixation applications.
- The corrosion rate of the Ti-Al-HA composite was significantly reduced to 0.003 mm/y.
- The Ti-Al-HA composite achieved a high relative density of 93%.

Keywords:

Powder metallurgy
Porosity
TiO_2
Hydroxyapatite
Corrosion resistance

ABSTRACT

The corrosion of implanted metals in the human body results in degradation and the release of harmful ions. Titanium and its alloys are used in biomedical applications due to their corrosion resistance and biocompatibility. This study examines how the amount of time spent sintering affects the density and corrosion resistance of Ti, Ti-6% Al, and Ti-6 % Al-2% HA (hydroxyapatite). Al was incorporated into Ti to reduce its density and enhance corrosion resistance. In contrast, HA was added at 2%, which aims to improve bioactivity and facilitate better integration with bone tissue. The samples were fabricated through powder metallurgy by mixing for 4 hours, and the compaction was 550 MPa. We sintered all samples at 1,300 °C, with varying sintering times of 60, 90, and 120 minutes. The results indicated that samples sintered for 120 minutes exhibited the highest relative densities: 91.55% for Ti, 92.89% for Ti-6%Al, and 93.24% for Ti-6%Al-2%HA. These samples demonstrated the lowest corrosion rates, with 0.2075 mpy for Ti, 0.01199 mpy for Ti-6%Al, and 0.003129 mpy for Ti-6%Al-2%HA. X-ray diffraction analysis of the Ti-6%Al-2%HA sample revealed patterns that corresponded to the titanium alloy and its byproducts, which included Ti, $CaTi_4P_6O_{24}$, TiP_2O_7, TiO_2, and $CaTiO_3$. Atomic absorption spectroscopy analysis found that only a small amount of titanium ions (0.912 ppm) was released, and no aluminum ions were detected over 14 days. Additionally, the MTT assay demonstrated 85.3% cell viability. These findings suggest that Ti-6%Al-2%HA alloys have potential applications in biomedical implants due to their improved corrosion resistance and biocompatibility.

1. Introduction

Titanium and its alloys, especially Ti-6Al-4V, have become foundational materials in biomedical engineering due to their remarkable biocompatibility, corrosion resistance, and mechanical properties [1–3]. These qualities have revolutionized implant technology and surgical procedures. However, challenges such as high production costs, mismatched elastic modulus compared to natural bone, and bioinert surfaces that hinder bone bonding continue to limit performance. Addressing these limitations has driven the development of novel material combinations and processing techniques.

Recent efforts in titanium alloy design have focused on enhancing strength and long-term performance while improving biological integration. Among the techniques employed, powder metallurgy (PM) has gained attention due to its ability to control composition and microstructure precisely, improving implant quality and healing efficiency [4,5]. Despite these advancements, the gap in current research lies in understanding how specific processing parameters, such as sintering time, affect the electrochemical and structural properties of titanium composites, especially those incorporating multiple modifying elements. Aluminum, commonly added to 6 wt.% to balance strength and plasticity, acts as an α-phase stabilizer. It also improves thermal stability and corrosion resistance by forming protective Al_2O_3 layers, though it can compromise ductility if used excessively [6,7]. Complementing this, incorporating bioceramic materials such as hydroxyapatite (HA) has significantly enhanced osseointegration and biological affinity [8]. HA's calcium-phosphate structure mimics

http://doi.org/10.30684/etj.2025.156810.1886
Received 11 February 2025; Received in revised form 04 May 2025; Accepted 23 May 2025; Available online 21 September 2025
2412-0758/University of Technology-Iraq, Baghdad, Iraq

natural bone, boosting tissue adhesion and promoting osteoconduction. Furthermore, combining HA with titanium alloys improves resistance to wear and corrosion while reducing the release of potentially inflammatory metal ions.

The synergistic properties of Ti-Al-HA composites have attracted increasing attention in biomedical materials science [9,10]. Processing methods and sintering parameters significantly affect the final microstructure and mechanical behavior. For instance, Omidi et al., fabricated pure titanium powder with HA using spark plasma sintering, varying the HA percentage from 0% to 40% in 2, 3, and 5 layers. The results demonstrated that grain size decreased as the HA content increased. However, vickers micro-hardness improved with increasing HA content, followed by a decline at higher HA levels. Maximum compressive strength was found in samples with five layers [11]. Farrahnoor and Zuhailawati, created a Ti-Nb-HA composite using mechanical alloying and powder metallurgy, investigating bioactivity with 0-15 wt.% HA. Increased HA content led to a decline in the β phase and the presence of α, TiO_2, and Ti_2P phases. The highest bioactivity was observed at 15 wt.% HA after immersion in Hank's Balanced Salt Solution (HBSS) for 30 days, with signs of HA decomposition improving bioactivity [12].

Li et al., developed Ti-6Al-4V/hydroxyapatite (HA) composites using selective laser melting, incorporating varying HA contents to form functionally graded materials (FGMs). Their findings demonstrated that incorporating 1 wt.% HA significantly enhanced osteogenic properties in vitro compared to higher concentrations or pure titanium. Furthermore, FGMs showed improved compressive strength while promoting bone tissue integration, indicating that a gradient distribution of HA can optimize both mechanical performance and biocompatibility of titanium-based implants [13]. Fereiduni et al., examined Ti-6Al-4V/HA composites made via Laser Powder Bed Fusion. Adding HA powder slightly enhanced reflectance compared to monolithic Ti-6Al-4V. Composites with 1 wt.% HA was crack-free, while those with 2.5 wt.% HA exhibited transgranular cracks. Adding 1 and 2.5 wt.% HA significantly improved nano hardness and yield strength [14]. α-stabilizing elements like aluminum increase the α-β transformation temperature in titanium. The addition of Al enhances mechanical properties and corrosion resistance due to the formation of an Al_2O_3 layer on the alloy's surface, as reported by Bolzoni et al. and Xu et al. in biomedical applications [15,16].

Despite such progress, limited studies have systematically explored the effects of sintering time on the density and corrosion resistance of Ti-based composites containing aluminum and HA. This research aims to fill this gap by evaluating Ti, Ti-6%Al, and Ti-6%Al-2%HA composites fabricated through powder metallurgy. By analyzing the relationship between sintering time and electrochemical properties, this study offers new insights for optimizing implant performance. Furthermore, it uniquely combines all three components—Ti, Al, and HA—in a single material system, contributing a novel perspective to biomedical material development.

2. Experimental work

2.1 Materials used

This study involves producing commercial pure titanium (CP), titanium-aluminum alloy (Ti-6%Al), and titanium-aluminum-hydroxyapatite composite (Ti-6%Al-2%HA) samples using powder metallurgy technology (P/M). These samples contain titanium in two different particle sizes (Ti1=484.9 nm, and Ti2=174.6 nm) with a mixing percentage of 70% Ti1 to 30% Ti2 (Using mixed coarse and fine particles improves density and reduces corrosion; fine particles fill voids, creating a compact structure, while smaller sizes enhance diffusion during sintering, improving bonding and corrosion resistance) [17]. The Al powder (6% by weight) is used as a liquid phase constituent, and HA (nano-powder, 2% by weight) is used as a bioactive constituent. Fluka, Swaziland, supplied the two titanium powder particle sizes (Ti1 and Ti2). Gientham Life Sciences Ltd., UK, supplied the aluminum powder. SUNKOO Ltd., Korea, provided the HA powder.

2.2 Work procedure

The experimental work involves the formation of 9 samples by powder metallurgy technology (P/M), which were divided into three groups depending on sintering times (Number 6 in each sample refers to 60 minutes, number 9 refers to 90 minutes, and number 12 refers to 120 minutes of sintering time) as shown in Table 1.

Table 1: Percentage of samples and their symbols

Group	Composition%	Symbol	Composition%	Symbol	Composition%	Symbol
60	100% Ti	T_6	Ti 6%Al	TA_6	Ti 6%Al 2%HA	TAH_6
90	100% Ti	T_9	Ti 6%Al	TA_9	Ti 6%Al 2%HA	TAH_9
120	100% Ti	T_{12}	Ti 6%Al	TA_{12}	Ti 6%Al 2%HA	TAH_{12}

2.3 Green compact preparation

Powder metallurgy (P/M) technology was employed to fabricate the samples through three main steps: mixing, compacting, and sintering. The samples obtained after compaction and before sintering are called green compacts. The weighed powders were mixed for 4 hours at a constant speed of 100 rpm. After mixing, the die of the final samples' required shape was prepared and lubricated with paraffin material. The mixed powders were manually distributed into the die cavity for optimum distribution before the next compaction step. Using a hydraulic press device at the University of Technology Materials Engineering Department, the powder is placed into the mold at 550 MPa for 15 minutes at a speed of 0.5 mm/s using a die and punch (1 cm^2 × 8.5 cm cylindrical cavity). Figure 1 (a, b) explains the mold and compaction process.

2.4 Sintering process

All samples (green compacts) were sintered in a furnace with a vacuum environment inside. The samples were distributed in three groups according to sintering time (60, 90, and 120 minutes) with a constant temperature average increase of 20 ˚C/min at (1,300 ˚C) as a constant temperature for all samples. Sintering at various times aims to select the best sintering time that gives the optimum properties (density and corrosion) for this work [18,19].

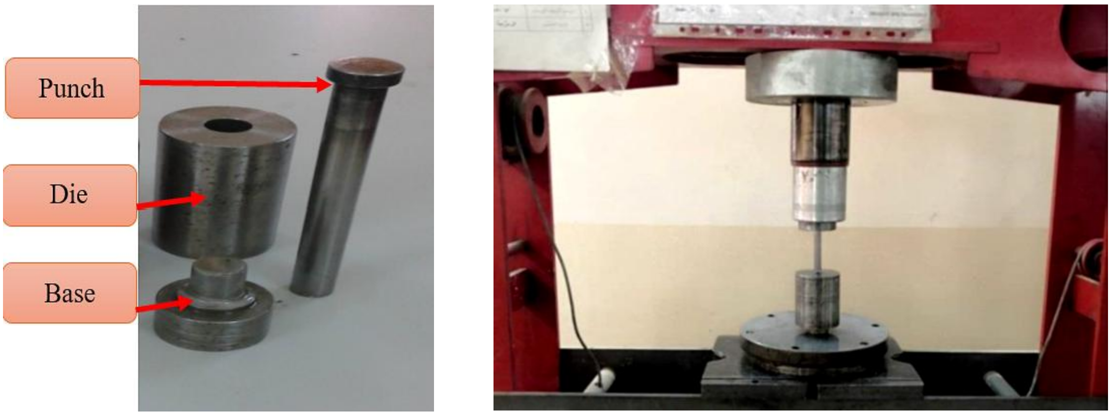

(a) **(b)**

Figure 1: a) The mold and b) compaction process

2.5 Density measurements

The apparent density, relative density, and porosity of each sample produced after sintering at various times were measured using the Archimedes method with a density measurement device in UOT\Materials Department\Chemical Library. The dry weight (W_{dry}) of each sample was measured. Subsequently, the samples were immersed in water for 24 hours to ensure saturation, after which the saturated weight in air ($W_{sat)}$ and the apparent weight while suspended in water (W_{sub}) were recorded. The apparent density (ρ_a) of each sample was then calculated according to the Archimedes method, following ISO 3369:1975 [20], as described in Equation (1). Density measurements were taken in triplicate for each sample to ensure the reliability and accuracy of the results. The average value of the three measurements was used for further analysis.

$$\rho a \; = \frac{\mathrm{Wdry}}{Wsat - Wsub} * \check{\mathrm{D}} \tag{1}$$

where: ρ_a: Apparent density (g/cm³), W_{dry}: Weight of the dry sample in air (g), W_{sat}: Weight of the water-saturated sample in air (g), W_{sub}: Weight of the saturated sample while suspended in water (g), ρ_{water}: Density of water (typically 1.0 g/cm³ at room temperature) [21].

The relative density ($\rho_{relative}$) of each sample was calculated according to Equation (2), while the theoretical density ($\rho_{theoretical}$) of each specific composition is 4.5 g\cm^3 for 100% Ti, 4.392 g\cm^3 for 94% Ti-6Al, and 4.3648 g\cm^3 for 92% Ti 6% Al 2% HA [22]. Finally, the relative porosity of each sample is determined according to Equation (3) [23].

$$\rho_{relative} = \rho_a \div \rho_{theoretical} \tag{2}$$

$$Relative\ Porosity = \left\{1 - \left(\frac{\rho relative}{\rho theortical}\right)\right\} * 100 \tag{3}$$

2.6 Corrosion measurements

Electrochemical corrosion tests were performed using a Corrtest CS350M Potentiostat/Galvanostat workstation at UOT/ Baghdad-Iraq\ Nanotechnology and Advanced Materials Research Center [24]. The samples had a cylindrical surface area of 1 cm² and a height of 0.5 cm. Each sample was insulated with Bakelite material; therefore, only one circular surface area was exposed to Ringer solution (simulated body fluid) with a 6.9 pH. They were grounded and polished using abrasive papers ranging from 100 to 4,000 grit to achieve a smooth circular surface area, as illustrated in Figure 2(a) [25]. A three-electrode cell was used to determine the electrochemical reaction parameters as illustrated in Figure 2(b). The corrosion cell consists of platinum, a pure metal (a secondary electrode), a saturated calomel electrode (a reference electrode), and the Ti-base samples (a working electrode) in the Ringer solution. A water bath was used to maintain the temperature of all experiments at 37 °C. This test is performed according to ASTM G10894 standard [26]. A scan rate of 1 mV/sec was used in this work to plot the Tafel curves (b_c and b_a), determining both the current density (i_{corr}) and the potential (E_{corr}). According to Equation (4), the corrosion rate (C.R.) can be calculated [26].

$$\mathrm{C.R} = \mathrm{C}\frac{M}{n\rho}\, icorr \tag{4}$$

where M: refers to the atomic weight (g/ mol), i_{corr}: refers to current density (A/cm^2), ρ: relates to density, C: refers to a constant equal to 0.13 in (mpy), and n: refers to the number of electrons involved in the process. The parameters of the corrosion test and their values of the operation are: Initial potential was -0.3V, Final potential was 0.3V, Frequency (Hz) was 2 Hz, and Scan Rate was 2 mV/s [27].

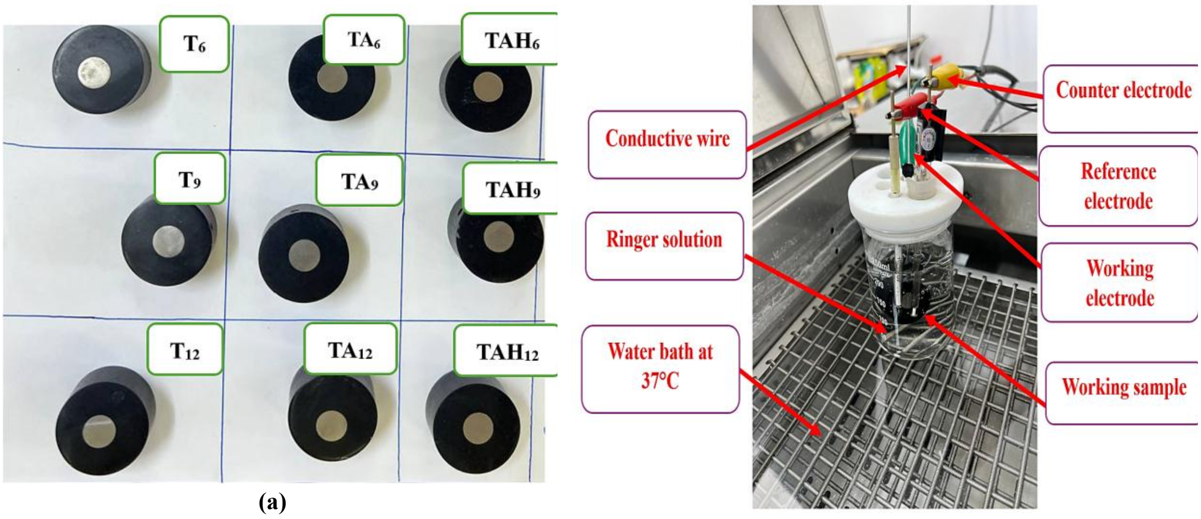

(a) **(b)**

Figure 2: a) Prepared samples for a corrosion test, and b)The corrosion cell

2.7 Atomic absorption spectroscopy measurements (AAS)

The optimum sample (according to corrosion resistance and relative density results of the three groups) was placed into a beaker (100 ml) containing a mimic bio-fluid substance (a Ringer solution). The optimum sample's Ringer solutions were prepared and evaluated for the AAS test at the Ministry of Industry and Minerals-Corporation for Research and Development, Ibn Al-Betar Center, Iraq. The beaker was incubated in a water bath at 37 °C, as shown in Figure 3(a). The Ringer solution was withdrawn from the beaker at three-, seven-, and fourteen-day intervals. This test determined the amount of ion release during the fourteen-day immersion period. Figure 3(b) shows samples of Ringer solutions at different periods: 3, 7, and 14 days.

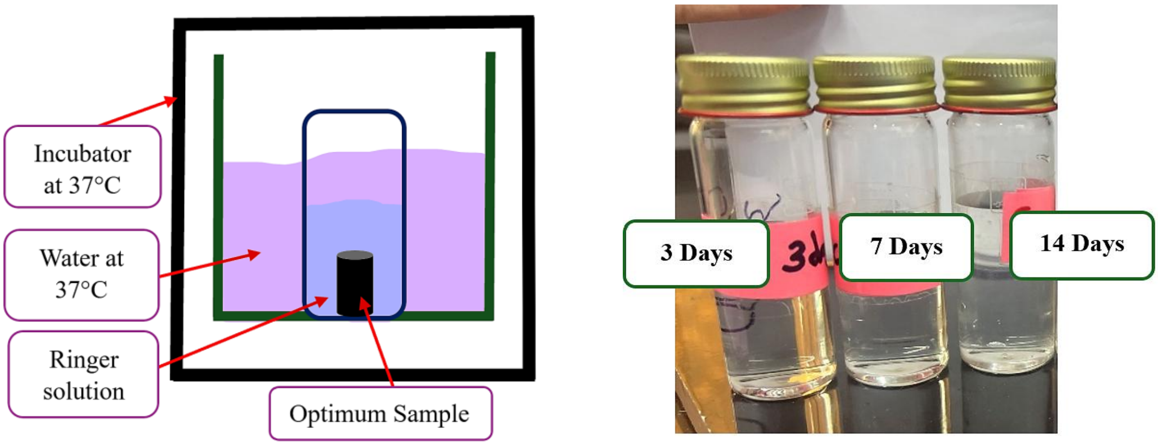

(a) **(b)**

Figure 3: a) Diagram of the AAS test and b) Ringer solution during different periods

2.8 MTT assay measurements

The chemical formula of MTT is (3- (4, 5- di-methyl-thiazol-2-yl) -2,5-diphenyl-tetrazolium bromide). The MTT assay, which uses yellow tetrazolium salt, was conducted at Shahrood University of Technology, Iran, to measure a cell's viability and cytotoxicity. In active cells, the soluble form of MTT is reduced to insoluble, purple formazan crystals. The amount of formazan can be measured spectrophotometrically at 550 nm after solubilization, and it is directly proportional to the number of viable cells. MG63 cells were cultured at 10^3 cells/well in 100 µL of culture medium, Dulbecco's Modified Eagle's Medium (DMEM), containing varying amounts of Ti-Al-HA powder in microplates (0.0001 µg/mL). The cell cultures were incubated for 24, 48, and 72 hours at 37 °C. After incubation, 10 µL of MTT reagent was added to each well. The microplate was then incubated for an additional 4 hours. 100 µL of Dimethyl Sulfoxide (DMSO) was added to each well. The plate was then incubated for 24 hours. The absorbance of each well was measured using a spectrophotometer at a wavelength of 550 nm. Control wells contained untreated cells, with an assumed relative viability of approximately 100% according to Equation (5). The mean absorbance of treated and control cells was calculated. Figure 4 illustrates the MTT test diagram [28].

$$Cell\ viability\ (\%) = \left(\frac{Mean\ absorbance\ of\ treated\ cells}{Mean\ absorbance\ of\ control\ cells}\right) * 100\% \qquad (5)$$

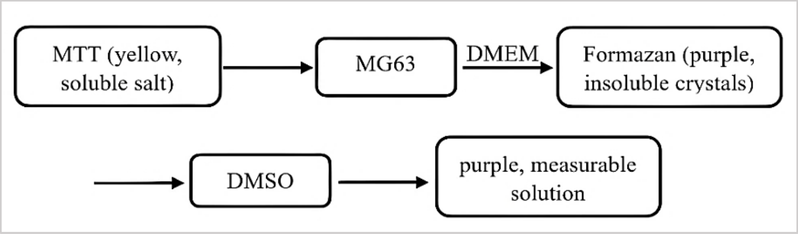

Figure 4: MTT assay chart

3. Characterization

An X-ray fluorescence (XRF) spectrometer, a powerful analytical tool designed to reveal the elemental composition of various materials, was utilized. A SPECTRO Analytic Instrument model (XEPOS) of 100 V was used to conduct this test. To determine the particle size of the powder, the 90Plus Particle Size Analyzer was employed. This device operates based on Dynamic Light Scattering (DLS), where it detects changes in the scattering of light, which are influenced by the random movement of particles within the suspension. By analyzing these fluctuations, the instrument provides precise data on the particle size distribution and the hydrodynamic diameter, both of which are crucial for evaluating the material's properties in various conditions. The Scanning Electron Microscope (SEM) device (Thermo Scientific Axia model) was employed to examine the specimen's surface morphology. The XRD test was performed using a Shimadzu X-Ray Diffractometer model XRD6000 to inspect the crystal structure of solid materials using X-ray beams.

4. Results and discussion

4.1 Particle size analysis

The examination resulted from charts Figure 5 (a- d) illustrating the value of effective diameter (d) for Ti_1 powder was 484.9 nm, for Ti_2 powder was 174.6 nm, for (Al) powder is 112.5 nm, and for (HA) powder is 72.5 nm and the distribution sizes had a slight span. The presence of different particle sizes (coarse and fine) in the sintered samples can lead to an increase in density compared to samples with only coarse particles. This improvement is due to the finer particles, which enhance interparticle necking growth during sintering. As a result, the porosity of the sample decreases, leading to a higher density [29].

4.2 X-ray fluorescence (XRF) analyzing

Figure 6 (a-d) presents the chemical analysis results for Ti1, Ti2, Al, and HA powders. XRF analysis indicates the purity of each powder, the elements detected as impurities, and their respective percentages. The analysis demonstrated that the purity of Ti1 powder is 98.89%, Ti2 powder is 98.78%, Al powder is 99.21%, and HA powder is 93.6%. These results confirm that the powders used to produce these alloys are pure. The XRF analysis of the received powders verifies the presence of the essential elements.

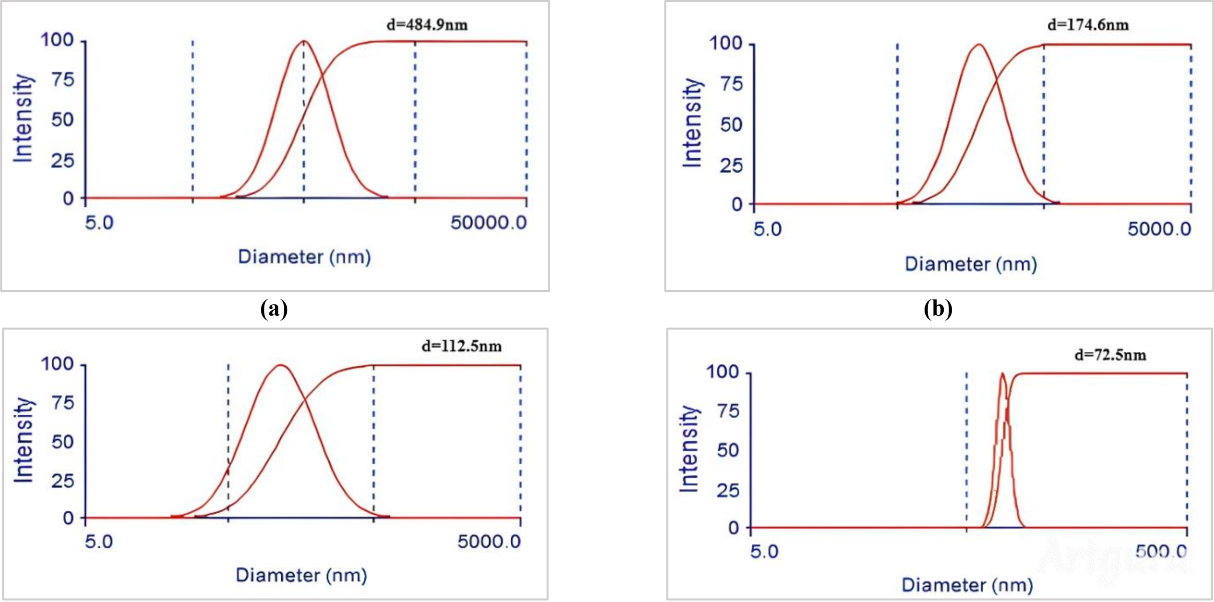

(a) (b)

(c) (d)

Figure 5: Particle size distribution diagram of a)Ti1, b) Ti2, c) Al and d) HA powders

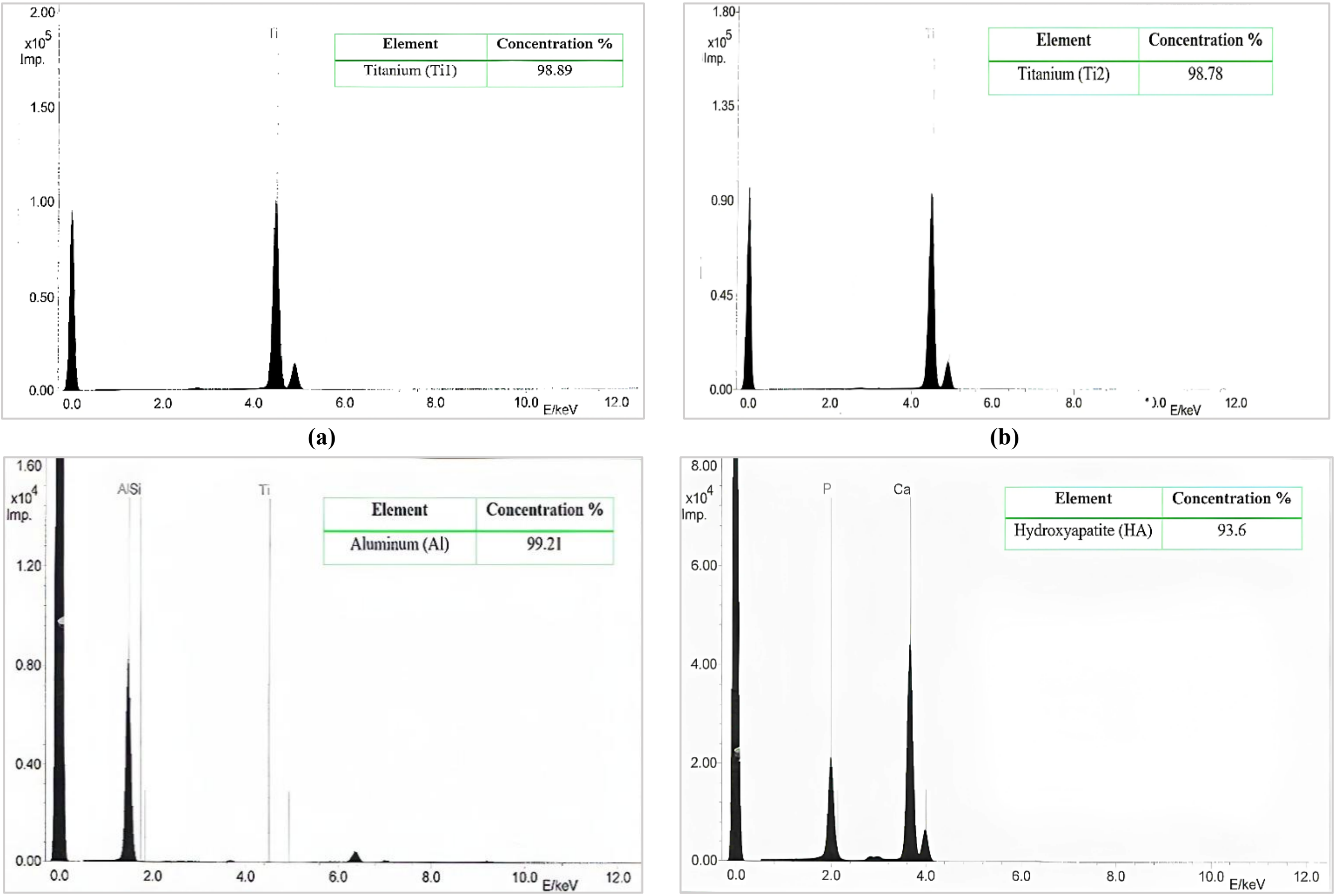

Element	Concentration %
Titanium (Ti1)	98.89

(a)

Element	Concentration %
Titanium (Ti2)	98.78

(b)

Element	Concentration %
Aluminum (Al)	99.21

(c)

Element	Concentration %
Hydroxyapatite (HA)	93.6

(d)

Figure 6: XRF results of a) Ti1, b) Ti2, c) Al, and d) HA powders

4.3 Density and porosity analysis

Table 2 shows the results of the density measurements. From this Table, the apparent density (g/cm^3), the relative density (%), and the relative porosity (%) of each sample are represented as a function of sintering times. Figures (7- 9) show that the apparent density and relative density gradually increase, while the relative porosity gradually decreases with the sintering times (60, 90, and 120 min) in this work. From Table 2, it can be observed that the lowest values of apparent density and relative density, and the highest values of relative porosity were recorded for samples sintered for 60 minutes. The apparent density and the relative density gradually increase, while the relative porosity gradually decreases as the sintering time is extended to 90 minutes for all compositions.

The maximum apparent density, the relative density, and the minimum relative porosity appeared at a sintering time of 120 minutes in all its specific compositions. The apparent density of sample T_{12} was 4.12 g/cm^3, for TA_{12} it was 4.08 g/cm^3, and TAH_{12} was 4.06 g/cm^3. The relative density of T_{12} was 91.55 %, for TA_{12} it was 92.89 %, and for TAH_{12} it was 93.24 %. The relative porosity of T_{12} was 0.796 %, TA_{12} was 0.788 %, and TAH_{12} was 0.786. The increase in relative density observed across all compositions (T_{12}, TA_{12}, and TAH_{12}) can be attributed to exposure to the highest processing time used in this study, compared to lower times of 60 and 90 minutes. This trend indicates a correlation between increasing sintering time and enhanced density. The sample TAH_{12} has the highest relative density because of the highest sintering time (120 min), the presence of Al and HA in its chemical composition, and this sample contains a variety of particle sizes (Ti1 is 484.9 nm, Ti2 is 174.6 nm, for Al is 112.5 nm, and HA is 72.5 nm). High sintering temperatures led to the closing of pores, reducing their total number, and causing them to adopt a spheroid shape [30-32]. Additionally, aluminum (Al) and hydroxyapatite (HA) brought the density of all samples closer to their theoretical values.

The presence of the Al element in titanium-based materials causes Ti to have an α-phase, which has a lower density than the β-phase Ti alloys. The Al element has a low density of about 2.7 g/cm^3, the HA has a theoretical density of 3.14 g/cm^3, and Ti has a density of 4.5 g/cm^3 [33]. The relative density results are adequate according to implants made of titanium-based materials, which are between 85-95% [34]. Materials with suitable porosity levels help minimize adverse biological reactions, such as inflammation, and promote healing. In metals like titanium, moderate porosity supports tissue adhesion while preserving mechanical integrity [35]. Their relative density significantly affects the corrosion resistance of biomedical titanium-based materials, particularly those produced through powder metallurgy. Higher porosity (which corresponds to lower relative density) increases the material's exposure to bodily fluids, thereby accelerating corrosion. Titanium alloys with moderate porosity can enhance tissue integration while maintaining sufficient corrosion resistance, particularly in orthopedic applications [36].

Table 2: Apparent density, relative density, and relative porosity results

Sintering Time (min)	Sample	Apparent Density (g/cm^3)	Relative Density (%)	Relative Porosity (%)
60	T_6	3.93	87.37	0.805
	TA_6	3.87	88.16	0.799
	TAH_6	3.86	88.25	0.797
90	T_9	3.97	88.22	0.803
	TA_9	3.91	89.02	0.797
	TAH_9	3.85	90.6	0.792
120	T_{12}	4.12	91.55	0.796
	TA_{12}	4.08	92.89	0.788
	TAH_{12}	4.06	93.24	0.786

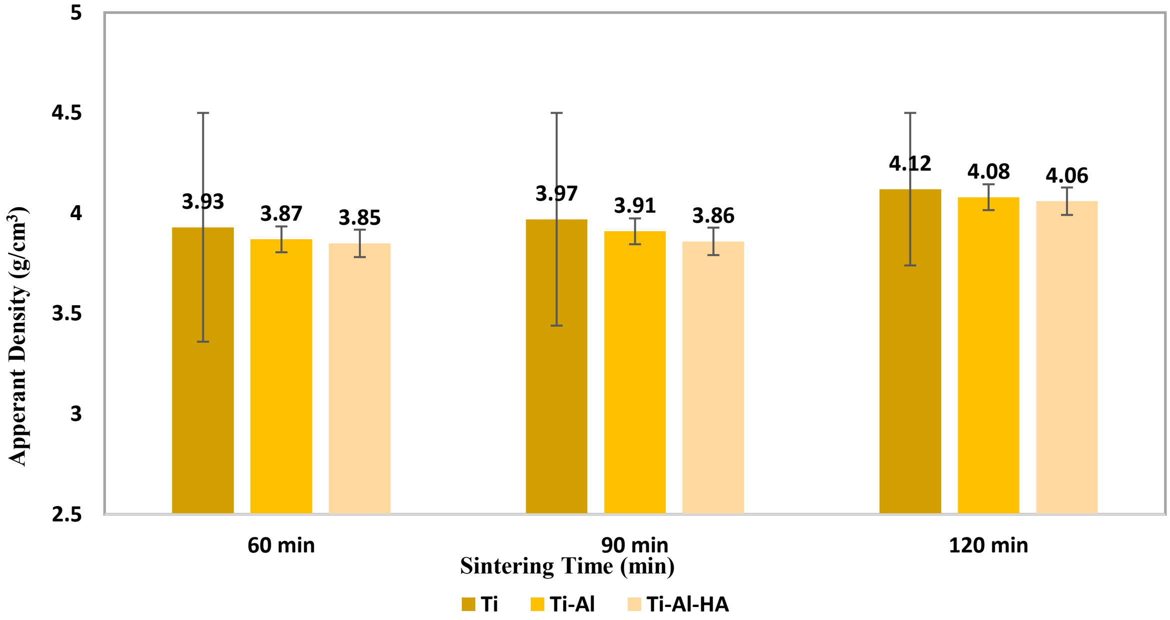

Figure 7: Effect of sintering times on apparent density

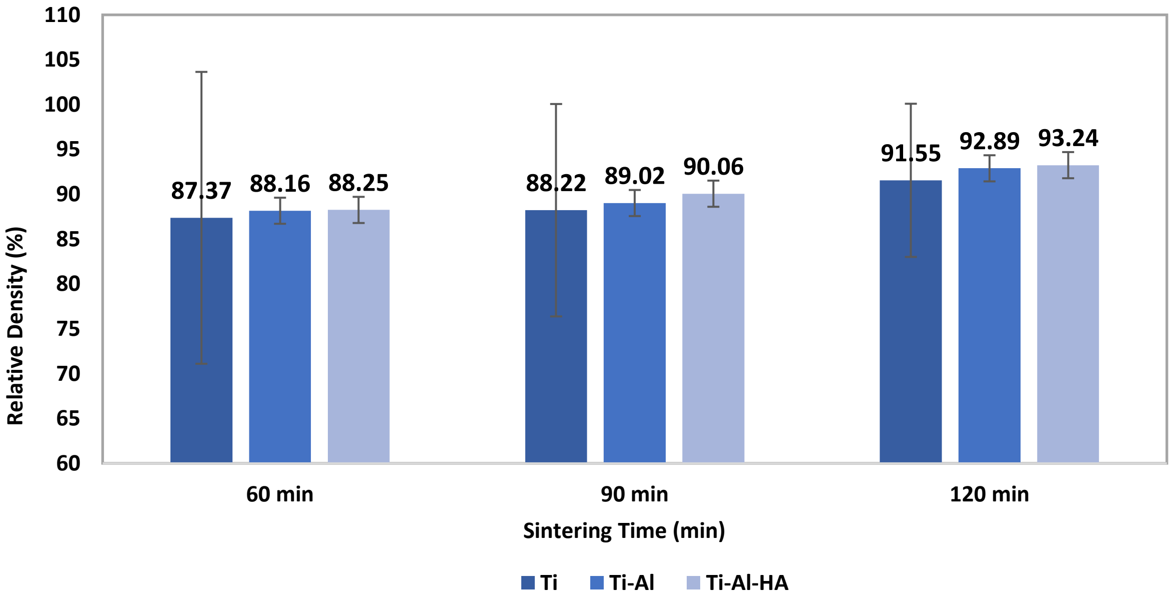

Figure 8: Effect of sintering times on relative density

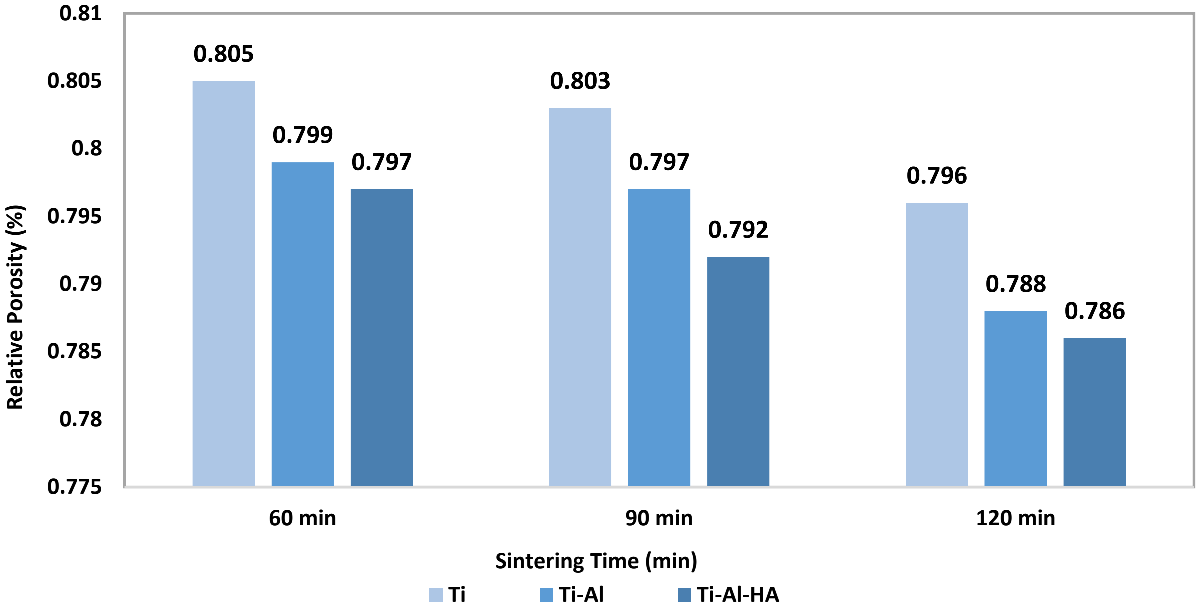

Figure 9: Effect of sintering times on relative porosity

4.4 Corrosion resistance analysis

Table 3 presents the results of the corrosion resistance evaluations, where the corrosion potential (E_{corr}) (V), corrosion current density I_{corr} (A/cm²), and corrosion rate (C.R.) (mm/y) are evaluated as a function of sintering time. The corrosion behavior of the samples was evaluated using the Corrtest CS350M Potentiostat. The device's ability to perform accurate electrochemical impedance spectroscopy (EIS) and potentiodynamic polarization allowed for precise corrosion potential and current measurement. These measurements provided reliable insight into the electrochemical stability of the Ti-based composites under simulated physiological conditions. Figures 10 (a-c) demonstrate the observed trends, with a progressive increase in the corrosion potential for all samples, which shifts significantly to the positive direction as the sintering time increases (60, 90, and 120 minutes). Conversely, the corrosion current density and rate decrease correspondingly, with the I_{corr} becoming more negative, under the same sintering conditions. The results show that the corrosion potential (E_{corr}) shifts notably to the positive side as sintering time increases. The corrosion current density (I_{corr}) decreases with longer sintering durations (increasing sintering time). Table 3 shows that the samples (T_6, T_9, T_{12}) exhibit corrosion rates (C.R.) of 0.3308, 0.2650, and 0.2075 mm/y, respectively. The corrosion rates in the TA6, TA9, and TA12 samples are lower than those of pure titanium (0.2320, 0.01854, and 0.01199 mm/y, respectively). Furthermore, when 6% aluminum is incorporated along with 2% hydroxyapatite into the titanium, a significant reduction in C.R. is observed in the TAH_6 and TAH_9 samples (0.02273 and 0.004854 mm/y, respectively), reaching the highest value in this study in the TAH_{12} sample, which is 0.0031298 mm/y. Figure 11 shows the corrosion rates of the samples in this work.

These results of TAH_{12} were due to the highest sintering time (120 min), which allowed for the highest relative density value (lowest relative porosity level), and using two different particle sizes of titanium powders compared to other samples with the same chemical compositions (TAH_6 and TAH_9). Furthermore, aluminum (Al) and hydroxyapatite (HA) presence in the chemical composition of sample TAH_{12} acts as a barrier against aggressive ion attacks, significantly enhancing the corrosion resistance of the Ti-Al-HA composite implant. An acceptable current density in titanium-based materials is typically less than 1 µA/cm². The low current density of Ti confirms that it remains in a passive state, thereby reducing corrosion risks. An acceptable corrosion rate is less than 1 µm/year (0.039 mm/y) [37-42].

Based on all samples' density and corrosion resistance test results, sample TAH_{12} exhibited the best performance as a biomaterial in this study. Consequently, further analyses were conducted on its microstructure, including SEM, XRD, AAS, cell viability assays, and cytotoxicity evaluation using the MTT assay.

Table 3: Corrosion potential (ecorr), corrosion current density (icorr), and corrosion rate (C.R.) results

Group	Sample symbols	E_{corr} (V)	I_{corr} (A/cm²)	C.R (mm/y)
60	T_6	-1.0745	2.8199E-05	0.3308
	TA_6	-1.0515	1.9779E-05	0.2320
	TAH_6	-0.98963	1.9381-06	0.02273
90	T_9	-1.0483	2.2593E-05	0.2650
	TA_9	-0.97341	1.5807E-06	0.01854
	TAH_9	-0.9934	4.138E-07	0.004854
120	T_{12}	-1.1111	1.7692E-05	0.2075
	TA_{12}	-0.96823	1.0222E-06	0.01199
	TAH_{12}	-1.0065	2.6679E-07	0.003129

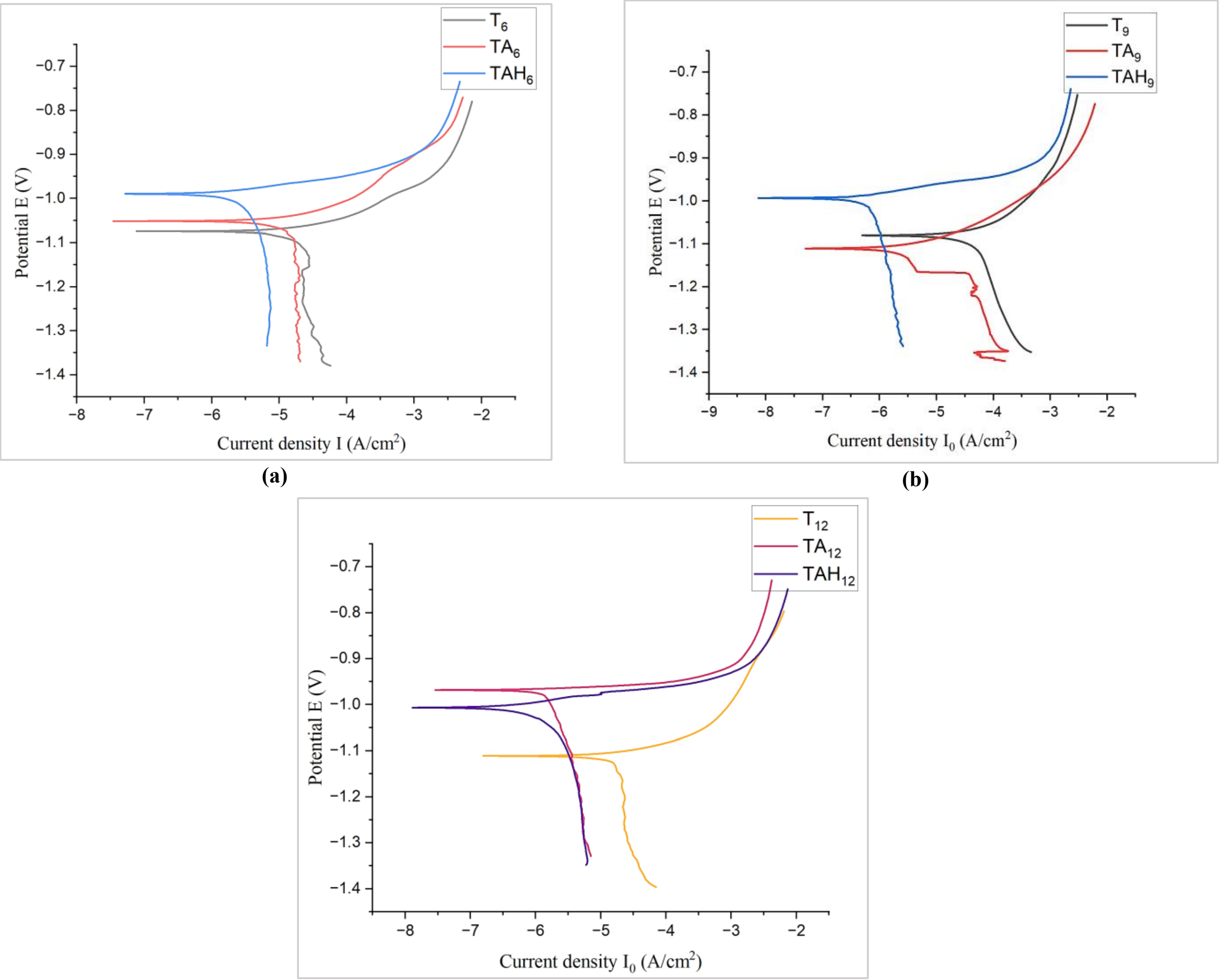

(a) (b)

(c)

Figure 10: a) Tafel curves of samples T_6, TA_6, and TAH_6. b) Tafel curves of samples T_9, TA_9, and TAH_9, and c) Tafel curves of samples T_{12}, TA_{12}, and TAH_{12}

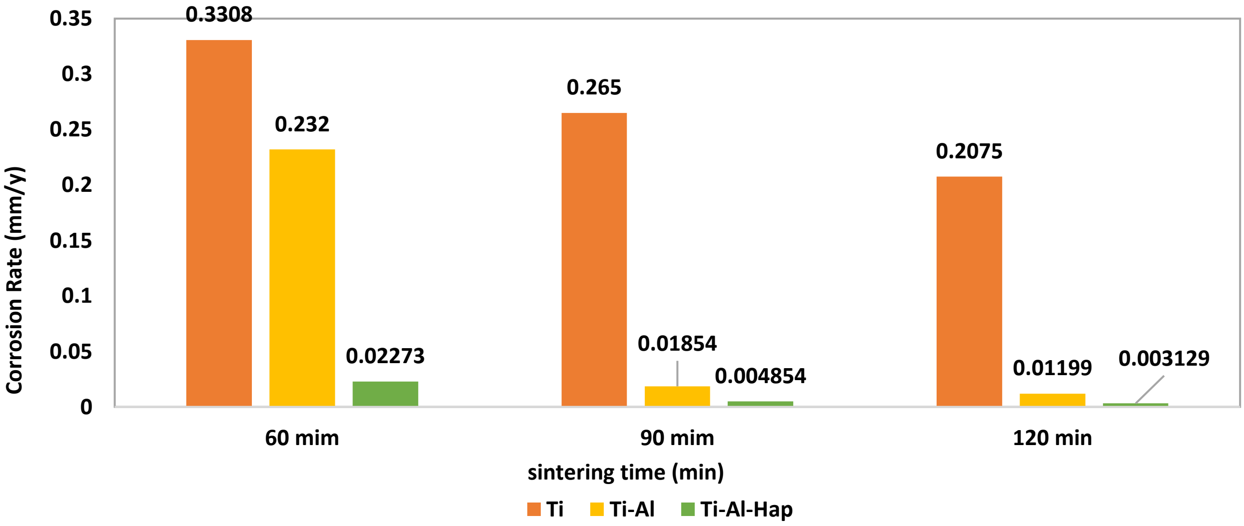

Figure 11: Corrosion rate analysis of samples

4.5 X-ray diffraction analysis

Morphological studies are significant and influential tools for surface characterization [43–45]. Sample TAH_{12} is produced from powders of 92% Ti, 6% Al, and 2% HA in weight by powder metallurgy processing with a sintering temperature of 1,300 °C and a sintering time of 120 minutes. The microstructural examination of sample TAH_{12} is shown in Figure 12. Multiple peaks indicate the formation of various compounds due to the decomposition of HA and its interaction with Ti and Al elements. These compounds include TiP_2O_7, Ti, Al_2Ti, $CaTiO_3$, TiO_2, $CaTi_4P_6O_{24}$, and $Na_2Ti_3O_7$. The standard reference cards for these compounds are displayed in Figure 12. Analyzing the presence of compounds formed after sintering titanium (Ti) with aluminum (Al) and hydroxyapatite (HA) at elevated temperatures, such as 1300 °C and a sintering time of 120 minutes, provides valuable insights into their potential effects on biocompatibility, mechanical properties, and stability within the context of biomaterials [46-50]. Including ceramic compounds in the TAH_{12} enhances its biocompatibility, making additional coating processes unnecessary.

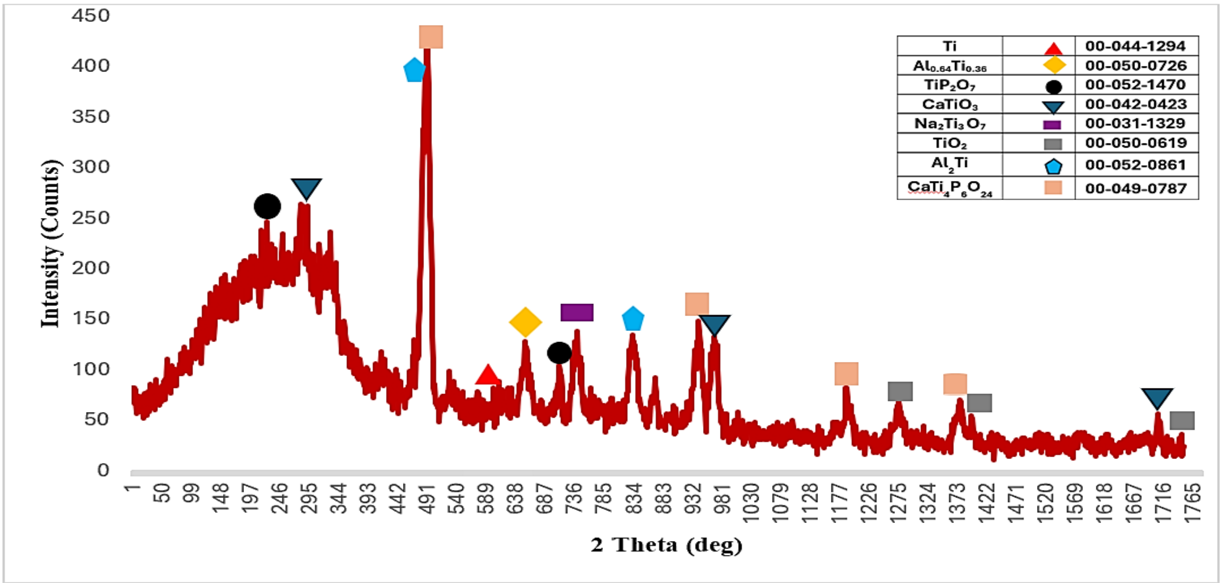

Figure 12: XRD analysis of TAH_{12}

4.6 Atomic absorption spectroscopy measurements (AAS) analysis

This study measured the ion release from the TAH_{12} sample in Ringer's solution. The maximum titanium ion release was 0.912 ppm, while aluminum ions were 0 ppm, as shown in Figure 13. Titanium, known for its non-toxicity, is naturally removed by the body and bonds well with bone if it is found in bodily fluids in amounts greater than 0.8 mg. Ion release stabilizes after a period due to adsorption processes, with various responses occurring on the implant surface when interacting with bone. Adsorption of metal ions is maintained by cell generation at the implant's surface, preventing further ion release [51, 52].

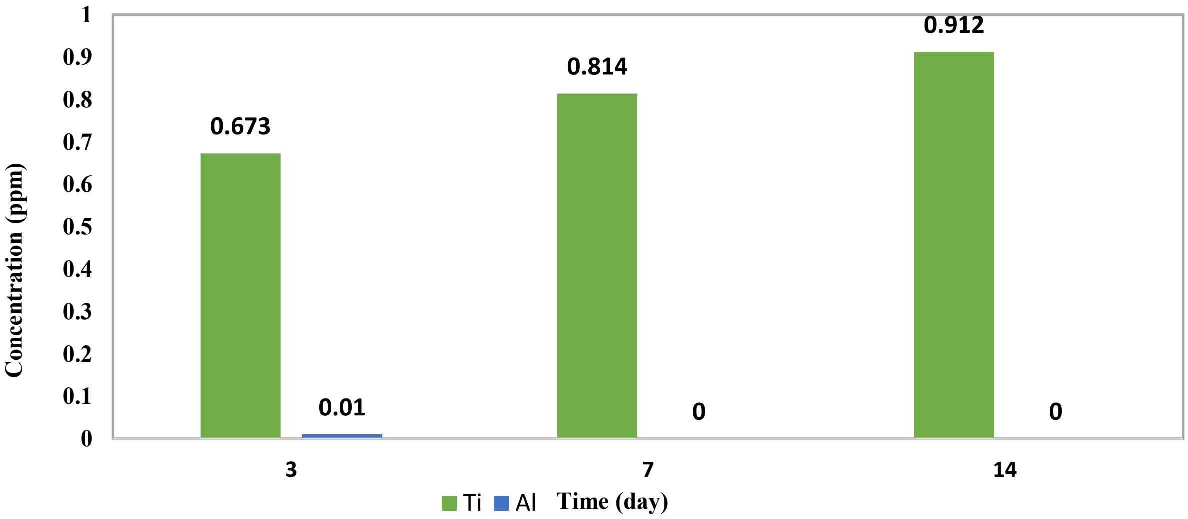

Figure 13: AAS test result of sample TAH_{12}

4.7 Scanning electron microscopy (SEM) analysis

Scanning Electron Microscopy (SEM) examination was conducted on the best sample (TAH_{12}) based on density and corrosion resistance results. This examination improved observations of surface morphology, as shown in Figure 14 (a and b), which displays the TAH_{12} sample at 50 µm and 5 µm, respectively. The particles and pores in this figure appeared in varied sizes and dimensions. The particles ranged from approximately 16 µm to 40 µm, while the pores were smaller than 5 µm. The SEM examination also revealed the homogeneity in particle sizes within the sample, contributing to its surface topographies. This surface homogeneity significantly impacts the surface roughness, playing a crucial role in the osseointegration of the implant and surrounding bone tissues [53]. Based on the SEM image shown in Figure 15 (a and b), the Roughness Average (R_a) of TAH_{12} was measured by the Gwyddion application. The roughness average of the TAH_{12} sample was found to be 73 nm. This result is attributed to the presence of nanoscale particle sizes in HA (72 nm) and Al (112 nm), along with the effect of high sintering time (120 minutes) at 1300 °C [54]. Incorporating nanostructured material on the implant's surface can enhance its performance. The nanostructured material produced a nano-rough surface (less than 1 µm). This nano-rough surface improves protein adsorption and cellular responses, leading to more dependable and faster osseointegration [54].

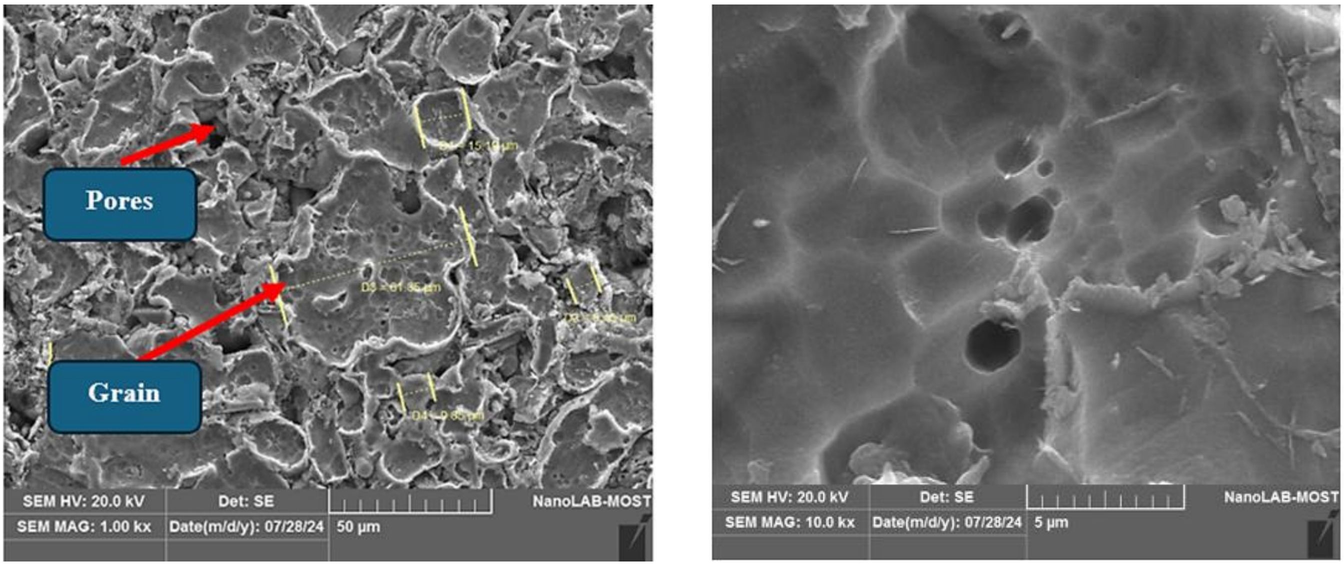

(a) **(b)**

Figure 14: The SEM of sample TAH_{12} at a) 50 µm, and b) 5 µm

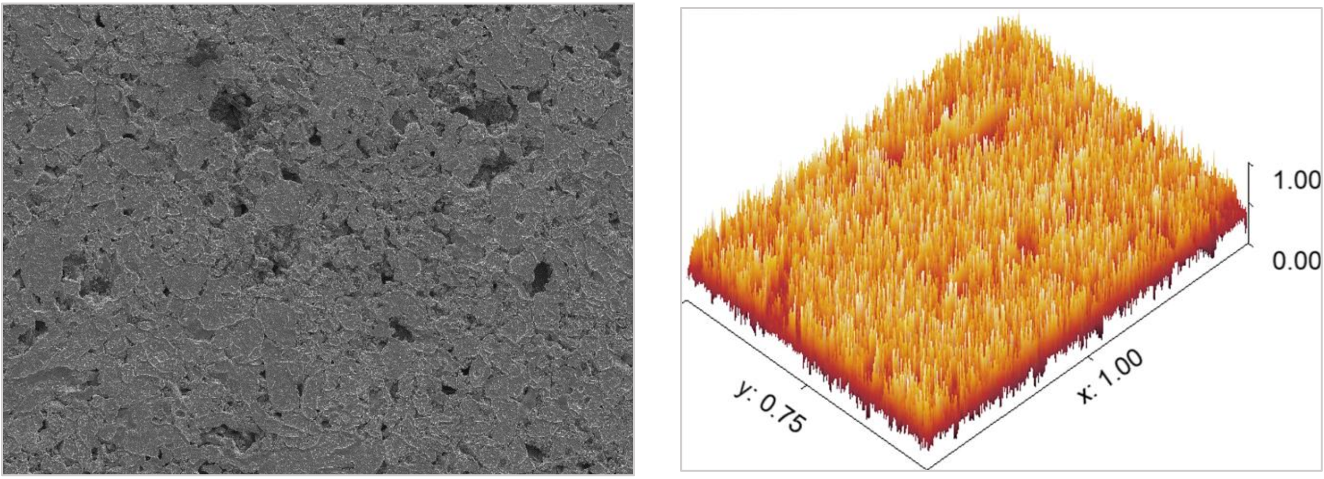

(a) **(b)**

Figure 15: a) SEM image at 200X, b) 3D image of SEM at 200X of sample TAH_{12}

4.8 MTT assay analyzing

When dissolved, formazan crystals show absorbance between 550–600 nm, with darker colours suggesting higher cell viability. Ti, Al, and HA materials are known to degrade slowly, releasing minimal ion concentrations, which are typically within acceptable safety limits and are considered to have low toxicity under established medical standards [55]. The highest recorded cell viability was 85.3% for cells cultured on the powder mix after 72 hours. The MTT assay revealed a cytotoxicity rate of 14.7%, which falls within the acceptable range for biomaterials (less than 30% cytotoxicity, as defined by ISO 10993-5:2009) [56], indicating moderate biocompatibility appropriate for preliminary evaluations Figure 16 (a and b). Titanium typically exhibits minimal tissue interaction due to its inert nature. While aluminium has been linked to health concerns like Alzheimer's disease with prolonged exposure, its reactivity in powder form can be mitigated. In this study, powder metallurgy sintering (1300 °C for 120 minutes) may have contributed to converting aluminium into a more stable crystalline phase, potentially reducing its long-term toxicity. Hydroxyapatite has been reported to support bone-implant bonding and promote osteointegration, potentially improving healing and reducing adverse responses [57–60].

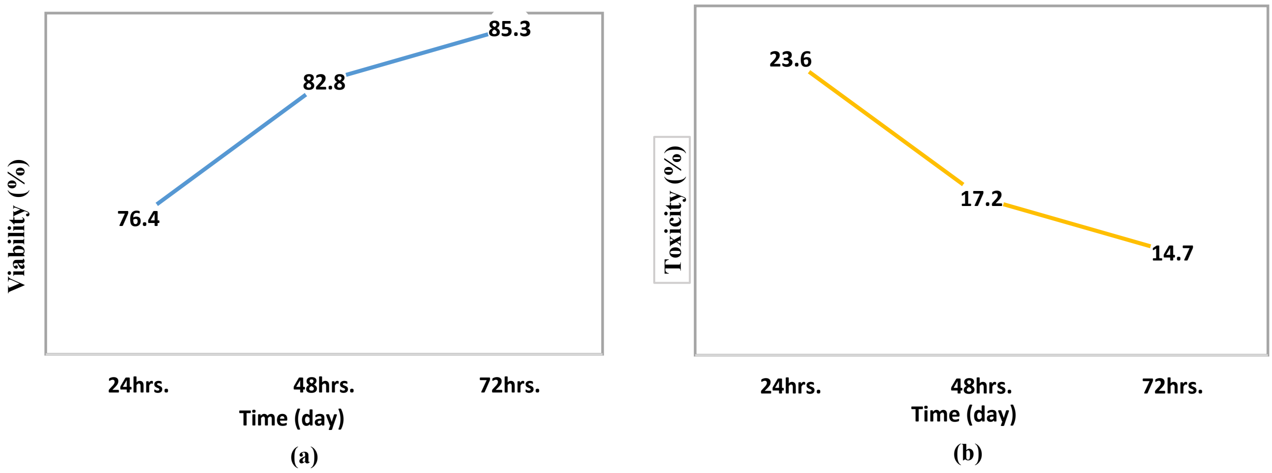

Figure 16: a) The cell viability with time, and b) The toxicity of the cell MG_{63}

5. Conclusion

This study explored the effects of varying sintering times (60, 90, and 120 minutes at 1300 °C) and particle sizes (484.9 nm and 174.6 nm) on the physical and corrosion properties of titanium-based alloys with different compositions: pure Ti, Ti-6%Al, and Ti-6%Al-2%HA. The results demonstrated that increasing the sintering time significantly enhanced the relative density across all compositions, with the highest value (93.24%) observed for Ti-6%Al-2%HA at 120 minutes. This improvement is attributed to the combination of smaller particle size and prolonged sintering, which promotes densification. In terms of corrosion resistance, Ti-6%Al-2%HA also exhibited the lowest corrosion rate (0.003129 mm/y) at the same sintering duration, outperforming pure Ti (0.2075 mm/y) and Ti-6%Al (0.01199 mm/y). The addition of HA played a crucial role by acting as a barrier against aggressive ions, while Al contributed to structural stability. XRD analysis revealed the formation of various compounds at higher sintering times, including TiP_2O_7, TiO_2, Al_2Ti, $Na_2Ti_3O_7$, $CaTi_4(P_6O_4)_6$, and $CaTiO_3$, indicating enhanced phase transformation and interaction at elevated thermal exposure. Overall, the study confirms that optimizing sintering time, particle size, and incorporating Al and HA can significantly improve titanium-based implants' density and corrosion resistance, enhancing their suitability for biomedical applications through improved biocompatibility and structural performance.

Author contributions

Conceptualization, **M. Hadi, N. Abdulkader, and L. Al-Gebory**; data curation, **M. Hadi**; formal analysis, **L. Al-Gebory**; investigation, **M. Hadi**; methodology, **M. Hadi**; project administration, **M. Hadi**, resources, **M. Hadi**; software, **N. Abdulkader**; supervision, **N. Abdulkader, and L. Al-Gebory**; validation, **M. Hadi**; visualization, **L. Al-Gebory**; writing—original draft preparation, **M. Hadi**; writing—review and editing, **M. Hadi**. All authors have read and agreed to the published version of the manuscript.

Funding

This research received no specific grant from any funding agency in the public, commercial, or not-for-profit sectors.

Data availability statement

The data that support the findings of this study are available on request from the corresponding author.

Conflicts of interest

The authors declare that there is no conflict of interest.

References

[1] R. Sridharan, A. R. Cameron, D. J. Kelly, C. J. Kearney, F. J. O'Brien, Biomaterial-based modulation of macrophage polarization: A review and suggested design principles, Mater. Today, 18 (2015) 313–325. https://doi.org/10.1016/j.mattod.2015.01.019

[2] D. D. Kiradzhiyska, R. D. Mantcheva, Overview of biocompatible materials and their use in medicine, Folia Medica, 61 (2019) 34–40. https://doi.org/10.2478/folmed-2018-0038

[3] X. Han, J. Ma, A. Tian, Y. Wang, Y. Li, B. Dong, X. Tong, X. Ma, Surface modification techniques of titanium and titanium alloys for biomedical orthopaedics applications: A review, Colloids Surf. B Biointerfaces, 227 (2023) 113339. https://doi.org/10.1016/j.colsurfb.2023.113339

[4] Z. Wang, Y. Tan, N. Li, Powder metallurgy of titanium alloys: A brief review, J. Alloys Compd., 965 (2023) 171030. https://doi.org/10.1016/j.jallcom.2023.171030

[5] Y. Mori , N. Mori, Advances in titanium alloys and orthopedic implants: new titanium alloys and future research directions, Bio-Des. Manuf., 7 (2024) 1053–1054. https://doi.org/10.1007/s42242-024-00314-1

[6] B. Wang, M. Luo, Z. Shi, Y. Cui, Y. Lv, C. Yang, L. Wang, Porous titanium alloys for medical application: Progress in preparation process and surface modification research, Materials Science in Additive Manufacturing, 3 (2024) 2753. https://doi.org/10.36922/msam.2753

[7] P. Barriobero-Vila, V. B. Oliveira, S. Schwarz, T. Buslaps and G. Requena, Tracking the α″ martensite decomposition during continuous heating of a Ti-6Al-6V-2Sn alloy, Acta Mater., 135 (2017) 132–143. https://doi.org/10.1016/j.actamat.2017.06.018

[8] Hench, L. L., and Wilson, J., An Introduction to Bioceramics; Advanced Series in Ceramics, World Scientific Publishing, University of Florida, 1993. https://doi.org/10.1142/2028

[9] E. S. Thian, J. Huang, S. M. Best, Z. H. Barber and W. Bonfield, Magnetron co-sputtered silicon-containing hydroxyapatite thin films—an in vitro study, Biomaterials, 26 (2005) 2947–2956. https://doi.org/10.1016/j.biomaterials.2004.07.058

[10] T. Masuda, M. Oh, and E. Kobayashi, Fabrication and Characterization of Biomedical Ti-Mg Composites via Spark Plasma Sintering, Materials, 17 (2024) 3470. https://doi.org/10.3390/ma17143470

[11] N. Omidi, A. H. Jabbari and M. Sedighi, Mechanical and microstructural properties of titanium/hydroxyapatite functionally graded material fabricated by spark plasma sintering, Powder Metall., 61 (2018). https://doi.org/10.1080/00325899.2018.1535391

[12] A. Farrahnoor, H. Zuhailawati, Effects of hydroxyapatite addition on the bioactivity of Ti-Nb alloy matrix composite fabricated via powder metallurgy process, Mater. Today Commun., 27 (2021) 102209. https://doi.org/10.1016/j.mtcomm.2021.102209

[13] Y. Lin, M. Balbaa, W. Zeng, Y. Yang, D. Mahmoud, M. Elbestawi, F. Deng, J. Chen, Osteogenic Properties of Titanium Alloy Ti6Al4V-Hydroxyapatite Composites Fabricated by Selective Laser Melting, J. Mater. Eng. Perform., 33 (2024) 9664–9675. https://doi.org/10.1007/s11665-023-08632-8

[14] E. Fereiduni, M. Balbaa, D. Mahmoud, M. Elbestawi, G. Li, J. Chen, & L. Yujing, Processing of hydroxyapatite (HA)–Ti–6Al–4V composite powders via laser powder bed fusion (LPBF): effect of HA particle size and content on the microstructure and mechanical properties. J. Mater. Res. Technol., 24 (2023) 8766–8781. https://doi.org/10.1016/j.jmrt.2023.05.111

[15] Froes, F. H., Titanium—Physical Metallurgy, Processing, and Applications, ASM Int.: Materials Park, OH, USA, 2015. https://doi.org/10.31399/asm.tb.tpmpa.9781627083188

[16] Y. Alshammari, B. Manogar, S. Raynova, F. Yang, L. Bolzoni, Behaviour of novel low-cost blended elemental Ti-5Fe-xAl alloys fabricated via powder metallurgy, J. Mech. Behav. Biomed. Mater., 110 (2020) 103865. https://doi.org/10.1016/j.jmbbm.2020.103865

[17] F. Qin, Q. Shi, G. Zhou, X. Liu, L. Chen, W. Du, D. Yao, Influence of Powder Particle Size Distribution on Microstructure and Mechanical Properties of 17-4 PH Stainless Steel Fabricated by Selective Laser Melting, J. Mater. Res. Technol., 25 (2023) 231–240. https://doi.org/10.1016/j.jmrt.2023.05.241

[18] S. V. Kumarán , J. M. Torralba, Development of competitive high-entropy alloys using commodity powders, arXiv preprint arXiv:2106.08576, (2021) 1–5. https://doi.org/10.48550/arXiv.2106.08576

[19] A. Rodriguez-Contreras, M. Punset, J. A. Calero, F. J. Gil, E. Ruperez, J. M. Manero, Powder metallurgy with space holder for porous titanium implants: A review, J. Mater. Sci. Technol., 76 (2021) 129–149. https://doi.org/10.1016/j.jmst.2020.11.005

[20] L. Bolzoni, E. M. Ruiz-Navas, E. Gordo, Understanding the properties of low-cost iron-containing powder metallurgy titanium alloys, Mater. Des., 110 (2016) 317–323. https://doi.org/10.1016/j.matdes.2016.08.010

[21] Lütjering, G. and Williams, J. C. Titanium; 2nd ed. (Berlin, Heidelberg: Springer, 2007. https://doi.org/10.1007/978-3-540-73036-1

[22] M. O. Bodunrin, L. H. Chown, J. A. Omotoyinbo, Development of low-cost titanium alloys: A chronicle of challenges and opportunities, Mater. Today: Proc., 38 (2021) 564–569. https://doi.org/10.1016/j.matpr.2020.02.978

[23] Callister, W. D. Jr., & Rethwisch, D. G., Materials Science and Engineering: An Introduction, 10th ed., Wiley, 2020. https://www.amazon.com/Materials-Science-Engineering-William-Callister/dp/1119721776

[24] Anaee, R. A. M. and Abdulmajeed, M. H. Tribocorrosion; Advances in Tribology, 2016. https://doi.org/10.5772/63657

[25] S. A. Naser, R. A. Anaee, H. A. Jaber and A. A. Khadom, Deposition of nickel-titanium coating on stainless steel 316L by direct current sputtering for bio-implants: Electrochemical, microstructural, and morphological investigations, Inorg. Chem. Commun., 165 (2024) 112478. https://doi.org/10.1016/j.inoche.2024.112478

[26] A. A. Azeez, Y. Danyuo and J. D. Obayemi, Effect of particle size and sintering time on the mechanical properties of porous Ti–6Al–4V implant, SN Appl. Sci., 2 (2020). https://doi.org/10.1007/s42452-020-2637-z

[27] Ratna, D. Recent Advances and Applications of Thermoset Resins; (2nd ed.). Retrieved from Elsevier, 2022. https://doi.org/10.1016/C2020-0-02814-8

[28] A. Van Tonder, A. M. Joubert and A. D. Cromarty, Limitations of the 3-(4,5-dimethylthiazol-2-yl)-2,5-diphenyl-2H-tetrazolium bromide (MTT) assay when compared to three commonly used cell enumeration assays, BMC Res. Notes, 8 (2015) 47. https://doi.org/10.1186/s13104-015-1000-8

[29] L, Reig, C. Tojal, D. J. Busquets and V. Amigo, Microstructure and mechanical behavior of porous Ti–6Al–4V processed by spherical powder sintering, Materials, 6 (2013) 4868– 4878. https://doi.org/10.3390/ma6104868

[30] M. B. Rahaei, D. Jia, M. Rahaei, H. Ghodrati, X. Duan, L. Zhao, H. Panahian, and A. Mohammadi, Manufacturing of high volume fraction of Ti_3AlC_2-Ti_2AlC metallic ceramics as nano-multilayered structures through high energy milling, hot pressing, and liquid phase sintering, Mater. Charact., 124 (2017) 1–12. https://doi.org/10.1016/j.matchar.2017.01.033

[31] S. A. Jabbar, N. J. Abdulkader, and P. S. Ahmed, Applying nanocomposite coatings to improve orthopedic alloys by using multiple flame spray, Eng. Technol. J., 41 (2023) 870–885. https://doi.org/10.30684/etj.2023.138886.1410

[32] S. A. Jabbar, N. J. Abdulkader and P. S. Ahmed, The investigation on properties of Ti-5Si and Ti-5Nb implant alloys coated by bioactive-based composite coating, Mater. Res. Express, 11 (2024) 036520. https://doi.org/10.1088/2053-1591/ad280a

[33] C. Veiga, J. P. Davim , A. J. R. Loureiro, Properties and applications of titanium alloys: A brief review, Rev. Adv. Mater. Sci., 32 (2012) 133–148.

[34] E. Marin and A. Lanzutti, Biomedical applications of titanium alloys: a comprehensive review, Materials, 17 (2024) 114. https://doi.org/10.3390/ma17010114

[35] R. Alkentar, N. Kladovasilakis, D. Tzetzis and T. Mankovits, Effects of pore size parameters of titanium additively manufactured lattice structures on the osseointegration process in orthopedic applications: a comprehensive review, Crystals, 13 (2023) 113. https://doi.org/10.3390/cryst13010113

[36] W. Xu, B. Zhang, C. Liu, and X. Qu, Effects of porosity on mechanical properties and corrosion resistance of PM-fabricated porous Ti-10Mo alloy, Metals, 8 (2018) 188. https://doi.org/10.3390/met8030188

[37] M. B. Radovanović, Ž. Z. Tasić, A. T. Simonović, M. B. Petrović, and M. M. Antonijević, Corrosion Behavior of Titanium in Simulated Body Solutions with the Addition of Biomolecules, ACS Omega, 5 (2020) 8260–8268. https://doi.org/10.1021/acsomega.0c00390

[38] M. Niinomi, Recent metallic materials for biomedical applications, Metall. Mater. Trans. A, 33 (2003) 477–486. https://doi.org/10.1007/s11661-002-0109-2

[39] T. Kokubo and H. Takadama, How useful is SBF in predicting in vivo bone bioactivity, Biomaterials, 27 (2006) 2907–2915. https://doi.org/10.1016/j.biomaterials.2006.01.017

[40] M. Moravej and D. Mantovani, Biodegradable metals for cardiovascular stent application: interests and new opportunities, Int. J. Mol. Sci., 12 (2011) 4250–4270. https://doi.org/10.3390/ijms12074250

[41] Y. Peng, C. Zhang, H. Zhou, L. Liu, On the bonding strength in thermally sprayed Fe-based amorphous coatings, Surf. Coat. Technol., 218 (2013) 17–22. https://doi.org/10.1016/j.surfcoat.2012.12.018

[42] C. Domínguez-Trujillo, F. Ternero, J. A. Rodríguez-Ortiz, S. Heise, A. R. Boccaccini, J. Lebrato, Y. Torres, Bioactive coatings on porous titanium for biomedical applications, Surf. Coat. Technol., 349 (2018) 584–592. https://doi.org/10.1016/j.surfcoat.2018.06.037

[43] W. Guo, Y. Wu, J. Zhang, S. Hong, G. Li, G. Ying, Y. Qin, Fabrication and Characterization of Thermal-Sprayed Fe-Based Amorphous/Nanocrystalline Composite Coatings: An Overview, J. Therm. Spray Technol., 23 (2014) 1157–1180. https://doi.org/10.1007/s11666-014-0096-z

[44] A. S. Dawood, A. A. Abdul-Hamead, and F. M. Othman, Preparation of Nano-alumina by green synthesis and study their structural properties, AIP Conf. Proc., 3002 (2024) 080018. https://doi.org/10.1063/5.0206458

[45] A. Arifin, A. B. Sulong, N. Muhamad, J. Syarif and M. I. Ramli, Material processing of hydroxyapatite and titanium alloy (HA/Ti) composite as implant materials using powder metallurgy: A review, Mater. Des., 55 (2014) 165–175. https://doi.org/10.1016/j.matdes.2013.09.045

[46] Y. N. Vaidyanath , K. G. Ashamanjari , K. R. Vishnu Mahesh , M. Mylarappa , M. S. Bhargava, et. Al., Development and characterization of titanium phosphates (tip_2o_7) and lithium titanium phosphate ($litip_2o_7$) and their thermal and electric properties, Int. J. Adv. Res., 13 (2025). http://dx.doi.org/10.21474/IJAR01/4797

[47] H. Onoda, T. Yamaguchi, Synthesis of titanium phosphates with additives and their powder properties for cosmetics, Mater. Sci. Appl., 3 (2012) 18–23. https://doi.org/10.4236/msa.2012.31003

[48] R. M. P. Colodrero, P. Olivera-Pastor, A. Cabeza, and M. Bazaga-García, Properties and applications of metal phosphates and pyrophosphates as proton conductors, Materials, 15 (2022) 1292. https://doi.org/10.3390/ma15041292

[49] A. J. Haider, Z. N. Jameel and I. H. M. Al-Hussaini, Review on: titanium dioxide applications, Energy Procedia, 157 (2018) 17–29. https://doi.org/10.1016/j.egypro.2018.11.159

[50] J. C. Ma, J. E. Benci and T. P. Feist, Effects of processing on the mechanical properties and oxidation behavior of Al_2Ti, MRS Proc., 364 (1994) 1303–1308. https://doi.org/10.1557/PROC-364-1303

[51] G. Senopati, R. A. R. Rashid, I. Kartika and S. Palanisamy, Recent development of low-cost β-Ti alloys for biomedical applications: a review, Metals, 13 (2023) 194. https://doi.org/10.3390/met13020194

[52] V. Suresh, A. K. Teja, and S. R. Gupta, Ion release dynamics of bioactive resin cement under variable pH conditions, Front. Oral Health, 6 (2025) 1564838. https://doi.org/10.3389/froh.2025.1564838

[53] Martins, J. R. S., R. O. Araújo, R. O. Araújo, T. A. G. Donato,V. E. Arana-Chavez, M. A. R. Buzalaf and C. R. Grandini, Influence of oxygen content and microstructure on the mechanical properties and biocompatibility of Ti-15 wt% Mo alloy used for biomedical applications, Materials, 7 (2014) 232–243. https://doi.org/10.3390/ma7010232

[54] G. R. Matos, Surface roughness of dental implant and osseointegration, J. Maxillofac. Oral Surg., 20 (2020) 1–4. https://doi.org/10.1007/s12663-020-01437-5

[55] A. Prokopchuk, I. Zozulia, Y. Didenko, D. Tatarchuk, and H. Heuer 1,3 and Y. Poplavko, Dielectric permittivity model for polymer–filler composite materials by the example of Ni- and graphite-filled composites for high-frequency absorbing coatings, Coatings, 11 (2021) 172. https://doi.org/10.3390/coatings11020172

[56] I. D. S. Brum, C. N. Elias, J. C. A. Lopes, L. Frigo, P. G.P. Dos Santos and J. J. De Carvalho, Clinical analysis of the influence of surface roughness in the primary stability and osseointegration of dental implants: study in humans, Coatings, 14 (2024) 951. https://doi.org/10.3390/coatings14080951

[57] International Organization for Standardization (1999), ISO 10993-5: Biological Evaluation of Medical Devices—Part 5: Tests for Cytotoxicity: In Vitro Methods. ANSI/AAMI. ISO 10993: Standards for the biologic evaluation of medical devices

[58] M. J. Mold, A. O'Farrell, B. Morris, C. Exley, Aluminum and Tau in Neurofibrillary Tangles in Familial Alzheimer's Disease, J. Alzheimers Dis. Rep., 5 (2021) 283–294. https://doi.org/10.3233/ADR-210011

[59] N. Jamal Abdulkader, P. Sahbah Ahme, S. Abduladheem Jabbar, Study the properties of Ti alloy by addition Nb and Si alloying elements for Orthopedic implant, J. Nanostruct., 14 (2023) 012115.

[60] A. Al-Ghaban, N. Jamal, H. Ahmed, Study on the Ti-C/nano-ceramic additives reaction due to sintering of elemental powders, J. Pure Appl. Sci., 31 (2019) 292–296. http://dx.doi.org/10.21271/zjpas